Electrochemical Growth of Pd for the Synthesis of Multiwall Carbon Nanotubes

ARTICLE *in* THE JOURNAL OF PHYSICAL CHEMISTRY C · JANUARY 2008

Impact Factor: 4.77 · DOI: 10.1021/jp077512l

Electrochemical Growth of Pd for the Synthesis of Multiwall Carbon Nanotubes

Rakesh K. Joshi,* Masamishi Yoshimura, Chien-Chao Chiu, Fa-Kuei Tung, and Kazuyuki Ueda

Nano High Tech Research Centre, Toyota Technological Institute Hisakata 2-Chome, Tempaku-Ku, Nagoya 4688511, Japan

Kei Tanaka

Daido Bunseki Research Inc., 2-30 Daido Minami-Ku, Nagoya 4578545, Japan

Received: September 18, 2007; In Final Form: November 3, 2007

Palladium nanostructures with variation in shape and size have been synthesized using an electrochemical deposition method. Cyclic voltammetry and linear sweep voltammetry have been used to study the growth of Pd nanoparticles on Si substrates and tungsten wire. Different sets of solutions containing $PdCl_2$, $Pd(NO_3)_2$, and $PdSO_4$, respectively, have been used to grow the Pd nanoparticles. Field emission scanning electron microscopy was used to visualize the Pd nanostructures on various substrates. The Pd nanostructures were used as a catalyst to grow the multiwall carbon nanotubes (MWCNT) by a microwave plasma enhanced chemical vapor deposition method. Dependence of the Pd nanoparticle shape on the architecture of MWCNTs is discussed. Carbon nanotubes were also grown on the tungsten tips. Development of Pd into Pd_2Si during growth of MWCNT on Pd-coated Si has been studied. The nanotubes were observed to be filled by Pd_2Si. Raman spectroscopy has been used to study the structure of the Pd_2Si filled carbon nanotubes.

Introduction

Architectural control of metal nanostructures is a field of immense interest for many applications. Properties of these metal nanostructures are determined by their size, shape, composition, crystallinity, and structure. Palladium (Pd) is one of the members of such class of metals that have been used as catalyst for various applications.[1−4] Pd has shown its potential for applications in various fields of engineering and technology including catalysis[1−4] and hydrogen storage.[5−10] Pd is one of the most used catalysts for the gas sensors[11−13] and has also been used as catalytic material for the synthesis of carbon nanotubes (CNTs).[2,14] Moreover, the carbon nanotubes loaded with Pd nanoparticles have been used for the detection of methane in the past.[15] Pd nanostructures with different shapes and sizes can make the surface occurring phenomenon more interesting. The application of Pd as a catalyst for the growth of carbon nanotubes can be extended for the purpose of making CNTs over the tips of scanning tunneling microscopy (STM) and atomic force microscope (AFM) that are made of tungsten (W) and silicon (Si), respectively, due to the availability of simple methods to make Pd nanoparticles on the given substrates. Several methods, e.g., physical and chemical, have been used to synthesize the metal nanostructures for various applications. However, a simple method to synthesize the Pd nanostructures in different structural forms with their direct application for the synthesis of carbon nanotubes is yet to be reported.

Electrochemical methods have been considered very useful for preparing the metal structures in the nanocrystalline form. A unique feature of electrodeposition is the ability to tune the orientation and morphology of electrodeposited films by controlling the nature of solution or the electrode overpotential. Critical control of growth parameters may lead to the formation of well-defined structures. Continuous research is going on to study the nucleation and growth of various metallic particles through electrodeposition processes. Reports are available on the growth kinetics of Pd films on various substrates through electrochemical routes using different ideas.[16−20] The results of such studies suggest that the shape and size of Pd nanoparticles are the function of cathodic over potentials. Metal nanoparticles with different shapes can be used for various catalytic applications. In our previous article,[21] we have reported, qualitatively, the synthesis of Pd nanoparticles on Si as a catalyst for CNT growth. In this article we study extensively the various aspects of electrochemical growth of Pd nanoparticles using different sets of electrolytes on Si as well as W substrates. Si and W were selected as the substrates considering the applicability in the field of fabricating CNT-attached scanning probe microscope tips. The issues regarding the identification of the materials filled inside the MWCNTs are likely to be solved in the present article.

Experimental Section

1. Synthesis. *(a) Pd Nanoparticles.* The Pd nanostructures were grown on Si substrate and W wires through potentiostatic electrodeposition using Hokuto Denko (HSV100) instrument. Three different sets of electrolytes were used for the growth of Pd nanoparticles. The first set of electrolyte consists of an aqueous solution of 0.04 mol/L $PdCl_2$ (50 mL) mixed with hydrochloric acid (10 mL); the second set consists of 0.04 mol/L $PdSO_4$ (50 mL) mixed with sulfuric acid (10 mL); the third set consist of 0.04 mol/L $PdNO_3$ (50 mL) mixed with nitric acid (10 mL). Some measured quantity of the electrolyte from one of the set was taken into an electrochemical cell for the growth of Pd nanoparticles on the chosen substrates. This process was repeated for another two set of electrolytes. The solutions were prepared using deionized water with specific resistance of 18

* To whom correspondence should be addressed. E-mail: rjoshi77@yahoo.com.

10.1021/jp077512l CCC: $40.75
Published on Web 01/17/2008

MΩ.cm. All the chemicals were supplied by Waco Chemicals Co. with a purity of more than 99%. A three-electrode configuration system was used for the growth of Pd nanostructures for the present study. The substrates were chemically cleaned using deionized water followed by cleaning with acetone using the ultrasonic agitator. Si substrates were additionally treated with HF solution for removing the native oxide layers. The cleaned Si substrates were dipped in electrolyte solution. In the case of chloride electrolyte, the solution is mixture of 50 mL of 0.04mol/L $PdCl_2$ plus 10 mL of HCl. The three electrodes were then dipped into the solution, and appropriate bias was applied to the system. After the chosen deposition time the substrates were taken out of the solution and dried. Once dried, they are ready to use for the growth of carbon nanotubes, thereafter, introduced into the MPECVD chamber for the CNT growth. A similar procedure was followed for the growth of Pd particles on W substrates.

(b) Carbon Nanotubes. The multiwall carbon nanotubes (MWCNTs) were grown on the Si substrates, which are coated electrochemically by Pd nanocrystals, using commercially available microwave plasma enhanced chemical vapor deposition (MPECVD) system (CVD-CN-100, Ulvac Japan Ltd.). The details of the instruments are described elsewhere.[22,23] A gaseous mixture of CH_4 and H_2 with a flow rate of 20 and 80 sccm, respectively, was introduced into the growth chamber, and the pressure was kept at 1.7 Torr for a growth time of 7 min. During growth, a voltage of −200 V was applied to the bottom electrode on which the substrate was mounted.

2. Characterization. Surface morphology of the electrochemically grown Pd nanostructures was investigated extensively using field emission scanning electron microscopy (FESEM, Hitachi S-4700). An energy dispersive X-ray system attached with SEM was used for the elemental analysis of the nanoparticles grown at different conditions. The growth kinetics of the nanoparticles deposited on different substrates was studied by cyclic voltammetry (CV) analysis. Crystallographic structure of the nanostructures grown on Si substrates was studied using glancing angle X-ray diffraction (GAXRD) and a high-resolution transmission electron microscopy (HRTEM), model JEOL JEM 2010, was used for microstructural study of carbon nanotubes. Structure of the MPECVD grown carbon nanotubes was investigated by Raman spectroscopy, model RENISHAW RAMASCOPE-2000, using an Ar ion laser at a wavelength of 514.5 nm.

Results and Discussion

1. Pd Nanoparticles. *(a) Growth.* The electrochemical deposition deals with the transfer of electrons from one substrate to another. This transfer creates a current with its magnitude giving information about the substance. Mechanism of electrochemical growth for the Pd nanoparticles has been studied using the voltammetry techniques. The CV that traces the transfer of electrons during a redox reaction that begins at a certain potential applied to the working electrode in a solution is discussed in detail. In CV the current in the cell is measured as a function of potential. The potential of an electrode in solution is linearly cycled from a starting potential to the final potential and back to the initial potential. The measurement in CV starts of with an initial potential followed by a specific potential. In the forward scan the electroactive species will start to get reduced, while in the reverse direction the oxidation process will take place. The potential that is cycled is the potential difference between the working electrode and reference electrode that was kept at a constant potential. If the potential is scanned monotically in one direction, then the voltammetry is known as linear sweep voltammetry (LSV), which is discussed later in this article.

Figure 1 shows CV plots for the growth of Pd nanoparticles on Si and W substrates for the three set of electrolyte solutions. The legends in the figures show the experimental conditions. A CV scan was performed in the negative voltage region for two cycles with a scan rate of 10 mV/s. The oxidation and reduction during the growth of Pd nanostructures can be easily seen from the peaks obtained for the case of Pd deposition on W wire substrate. For the W wire substrate, the CV scan shows separate potential region for both the measured cycles unlike the CV scan for Pd growth on Si substrate. In the case of Si, we have not found the peaks in measurement range. The CV was performed only for the voltage from a very small positive value that is close to zero as shown in the figure to a negative value of approximately −1.5 V. It is possible that the peaks can be obtained for higher negative voltages. Since the films were deposited at lower voltages, therefore, the CV was not studied at higher negative voltages than that shown in Figure 1 in the case of Si, while, in case of W we obtained the peak at very lower negative voltages. Repeated voltammetry measurements show the results similar to the above-discussed behavior.

In case of W wire substrates the values of the cathodic peak potential (E_{pc} = voltage at which the current is highest), highest current value (I_{pc}), anodic peak potential (E_{pa} = the voltage at which current is minimum), and minimum current value (I_{pa}) can be seen from the plots for the W wire substrate. The anodic current peak (E_{pa}) can be seen in the second cycle as well as in the first cycle, with an increasing depth in the second cycle. This shows that a reversible process, which is reduction of Pd^{2+} to Pd^0, has taken place on the surface with an incomplete reduction process indicating the availability of reacting ions for further deposition. Anodic and cathodic peaks are observed in the voltammograms with values of I_{pc} and I_{pa} of nearly equal magnitude for the different cycles, respectively, in the case of W wire substrates. It shows a less possibility of charge trapping inside the films and it can be said that the growth has good reversibility. Under these conditions the peak current, I_p, is expressed by the Randle−Sevcik relationship

$$I_p = kn^{3/2}AD^{1/2}CV^{1/2}$$

Where the constant, k, has a value of 2.72×10^5, n is the moles of electrons transferred per mole of electroactive species, A is the area of the electrode in cm^2, D is the diffusion coefficient in cm^2/s, C is concentration in mol/L, and V is the scan rate of the potential in V/s. The peak current, I_p, is linearly proportional to the bulk concentration, C, of the electroactive species and the square root of the scan rate. Thus, an important diagnostic is a plot of the I_p vs scan rate$^{1/2}$. Figure 2 shows plot for I_{pa} vs scan rate$^{1/2}$ for the electrochemical growth from chloride electrolyte solution on the W wire substrates. I_{pa} values were taken after only 1 electrochemical cycle and thus with incomplete reduction. Electrochemical reaction was carried out at four different values of scan rates, 100, 10, 1, and 0.16 mV/s for studying the variation of peak current with scan rates. The experimentally observed linear behavior for the plot I_{pa} vs scan rate$^{1/2}$ suggests that the electrode reaction is controlled by diffusion, which is the mass transport of electroactive species to the surface of the electrode across a concentration gradient. The change in the slope of the line indicates the change of diffusion coefficients. This analysis was also performed for the other two electrolytes, namely, the sulfate and nitrate, and the observed linear behaviors for the plot I_p vs $V^{1/2}$ suggested the

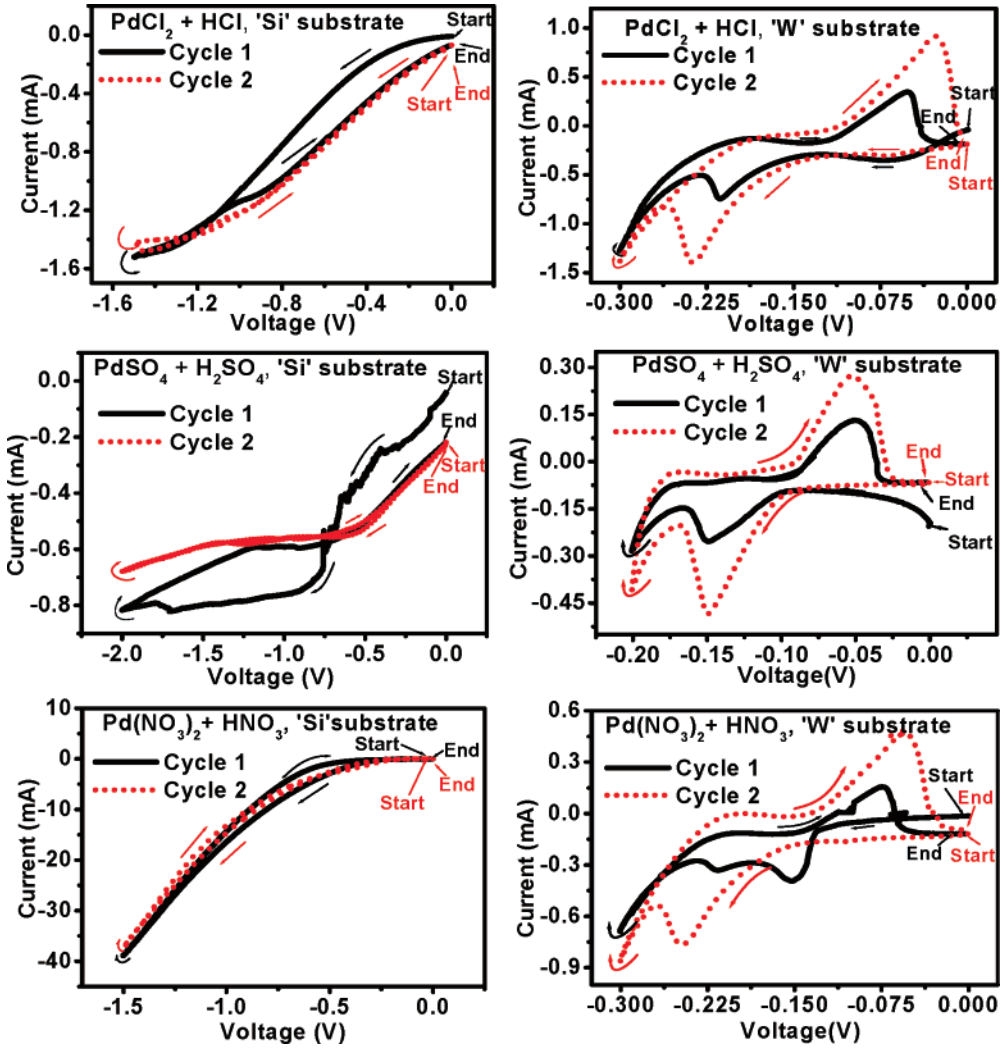

Figure 1. CV plots for the growth of Pd nanoparticles on Si and W substrates for the three set of electrolyte solutions.

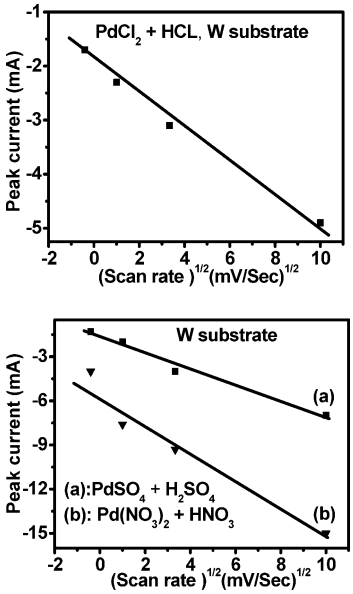

Figure 2. Plots for peak current (I_{pa}) vs scan rate$^{1/2}$ for the electrochemical growth on the W wire substrates. I_{pa} values were taken after only 1 electrochemical cycle.

occurrence of diffusion-controlled reactions during the growth of Pd nanoparticles on W substrate from the discussed electrolyte solutions.

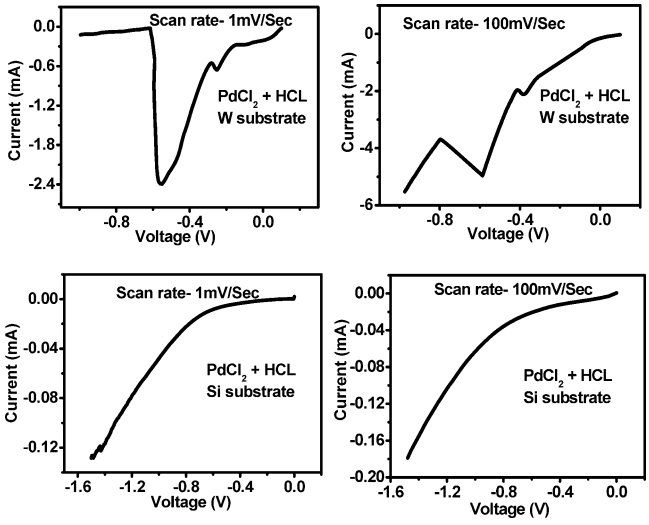

Figure 3. Plots for LSV during the growth in W wire and Si substrates for the chloride electrolyte solution at scan rates of 1 mV/s and 100 mV/s.

LSV studies were carried out for the growth of nanoparticles. Figure 3 shows the typical plots for LSV during the growth in W wire and Si substrates, for the chloride electrolyte solution. Change in the value of I_{pa} with scan rate can be seen from the plots for growth on W wire for the two values of scan rates, i.e., 1 and 100 mV/s. The LSV was carried out for four different

values of scan rates, which are 100, 10, 1, and 0.166 mV/s. Each curve has nearly the same form, but it is apparent that the total current increases with increasing the scan rate. This can be rationalized by considering the size of the diffusion layer and the time taken to record the scan. Clearly, the linear sweep voltammogram will take longer to record as the scan rate is decreased. The size of the diffusion layer above the electrode surface depends on the voltage scan rate used. In slow voltage scan, the diffusion layer grows much further from the electrode in comparison to the fast scan, and the flux to the electrode surface is considerably smaller at slow scan rates than in the case of faster rates. Since the current is proportional to the flux toward the electrode therefore, the magnitude of the current will be lower at slow scan rates and higher at high rates. The voltage scan rate does strongly affect the LSV behavior. It can also be noted from the above LSV results that the position of the current maximum appears nearly at the same voltage for different scan rates. This is a characteristic of electrode reactions that have rapid electron-transfer kinetics. These rapid processes are known as the reversible electron-transfer reactions. On associating the CV and LSV measurements it is seen that the voltage range of experiments for both the studies is nearly the same in the case of Si (Figure 1 and 3), while in the case W, the LSV was done over a large votage range in order to see the current maximum peak clearly. The current maximum peak was not observed in the case of Si, but in the case of W this peak was observed, and therefore the voltage range was extended more than the CV voltage range, in order to see the peak completely.

(b) Surface Morphology and Structure. Pd nanostructures of different shapes and sizes were grown on the Si substrates and W wires. For the preparation of the first set of samples a mixture of 0.4 mol/L $PdCl_2$ and HCl was used as electrolyte. Detailed SEM observations were performed on these samples to visualize the shape and size of the nanoparticles. The morphological similarity of the Pd particles grown on Si and W substrates is that the Pd nanoparticles follow a nonspherical growth for both type of substrates at nearly all the selected growth conditions for the above-mentioned chloride electrolyte solutions. Clearly, the triangular-shaped nanoparticles were observed to be the elementary structures of Pd on the Si substrate, wheareas the nanospikes were observed to be the building blocks for the Pd nanostructures on the W wires under the similar growth conditions. The size of nanotriangles on Si substrate can be varied by changing the applied potential to the working electrode, whereas the shape of these nanoparticles can be tailored by varying the deposition time. Higher voltages lead to the nanostructures of a bigger size for a fixed deposition time. The variation in the shapes of Pd nanostructures with time has been shown in our earlier report.[21]

The Pd nanostructures follow a triangular-shaped particle growth on the Si substrates and spike shaped particle growth on W substrate. It has been seen that the structures on Si grow initially as triangles followed by cubes in the overgrowth conditions on increasing the deposition time and star-shaped Pd nanostructures "nanostars" for further increase of deposition time to some higher value (~20 min) for a fixed bias applied to the working electrode.[21] The possible mechanism for such a change in morphology of Pd nanoparticles on Si substrates has been proposed.[21] The SEM micrographs showing the nanotriangles, nanocubes, and nanostars on the Si surface have been presented in our earlier report.[21] It has been discussed that the application of a bias voltage of 0.01 V for a deposition time of 5 min produces triangular structures in higher density than the cubes and stars on the Si substrates, whereas the cubes are in the higher majority for the deposition time of 10 min followed by the highest number of nanostars on further increasing the deposition time to 20 min.

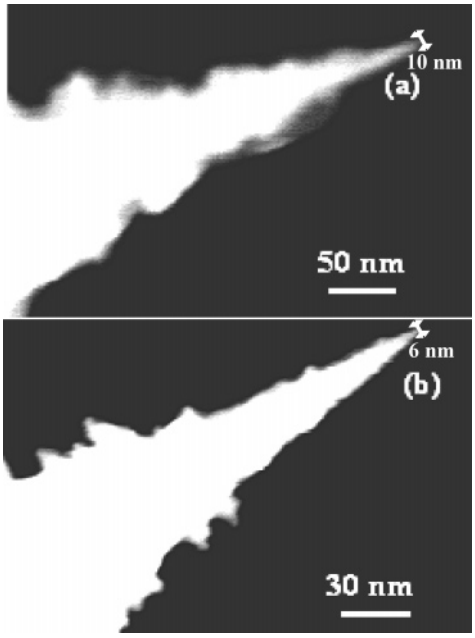

Figure 4. FESEM micrographs for the nanospike grown on W wire at 0.25 V (a) and 0.1 V (b) for a deposition time of 5 min using an electrolyte solution, which is a mixture of $PdCl_2$ and HCl.

In W wire substrates the typical shape for nanoparticles is a spike. Figure 4 shows the decrease in the diameter of the nanospike grown on W wire at 0.25 V (a) and 0.1 V (b) for a deposition time of 5 min using an electrolyte solution that is a mixture of $PdCl_2$ and HCl. On the basis of the SEM study made on the series of samples grown on W wire, it is suggested that the size and width of these nanospikes can be varied by changing the applied voltage to the working electrode.

Parts a and a′ of Figure 5 show the SEM micrographs for the comparative study of structures grown on Si and W wire of 0.3 mm thickness using the $PdCl_2$ electrolyte. It is seen that the nanotrianlges accompanied with nanocubes and nanostars were obtained on the Si substrates, whereas the nanocubes accompanied by ball-bearing nanospikes were obtained on the W wire as shown in Figure 5a′. This is to mention that the Pd particles with nanocube shape were observed for both types of substrates. The growth of Pd nanostructures as the ball bearing spikes coupled with cubes was observed by growing the films for a very short deposition time. It is noticed that the structures are mostly cubes at the smooth surface of W wire and ball-bearing nanospikes at the rough surfaces. The roughness in the W wire is expected due to its unpolished surface. We believe that the rough surface on the W wire guides the growth in the form of a spike, whereas the smooth surface gives the cubes. This discrimination in shape of nanoparticles (cubes and spikes) grown on W substrates for the same solution occurred most probably due to the presence of native oxide in the W substrate, which, up to some extent, guides the growth at uneven and disordered places. Here, we must note the analysis of Bera et al.[24] for the growth of Pd nanoparticles. They have reported the formation of Pd nuclei on the surface of stainless steel by electrodeposition and suggested that the nucleation initially occurs at the holes or disorder state of the substrate on which the metal is to be deposited. Following their analysis, the reason for above-mentioned discrepancy in shape of nanoparticles on W wires can be attributed to the uneven nature of the substrate

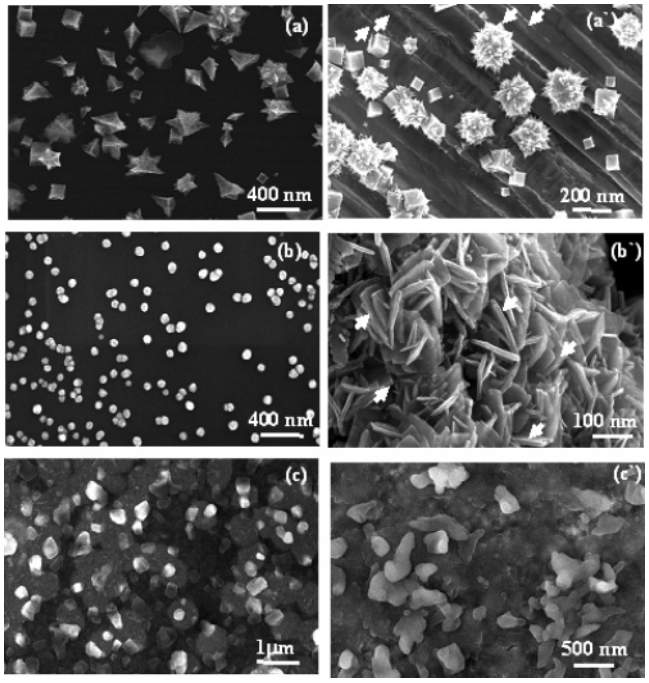

Figure 5. FESEM micrographs for the structures grown on Si (left) and W wire (right) using $PdCl_2$ + HCl (a), $PdSO_4$ + H_2SO_4 (b), and $Pd(NO_3)_2$ + HNO_3 (c) electrolytes.

surface and presence of oxide, which is more probable at the grain boundaries or at the disordered place. It is worthy to note that the formation of W oxide can take place easily at room temperature that is energetically more favored at the disordered state due to the presence of defects. Therefore, instead of a continuous deposition throughout the surface of the W with particles of the same morphology, a localized deposition took place with discrimination in the shape of nanoparticles.

To summarize the above results we say that the nature of the surface of the substrate at working electrode has a dominant effect in deciding the shape of the nanostructures grown by electrochemical deposition technique. Verification of this substrate surface effect on the shape determination of nanostructures can be seen by comparing the morphology of the Pd nanoparticles grown on Si substrate with the Pd nanoparticles grown on W wire. We have observed well-defined cubes, triangles, and stars on the Si surface with no spikes/ball-bearing spike, which have been understood to be generated because of the surface roughness of the substrate. The elementary shape in case of deposition on the Si surface is a triangle, where the two triangles are giving a cube and multiple triangles are resulting into the stars; therefore, the localized deposition could not be ruled out even on the smooth Si surface; however, it was controlled up to little extent in comparison of the case of deposition on the W surface.

To achieve more variation in the shape of Pd nanostructures, a different set of electrolytes other than the above-mentioned chloride electrolyte were used. Surface morphology of the nanoparticles grown under such conditions was studied by FESEM. Spherical nanoparticles with nearly monodisperse quality (Figure 5b) have been obtained on the Si substrates on using the electrolyte that is a mixture of 0.04 mol/L $PdSO_4$ and H_2SO_4, whereas the Pd structures with the shape of a nanosheet were obtained on the W wire substrate using the sulfate electrolyte. The nanosheets are marked by a white arrow to show them clearly in Figure 5b′. Average dimensions for the nanosheets were calculated using various SEM pictures including the cross-sectional view. The nanosheets have an average

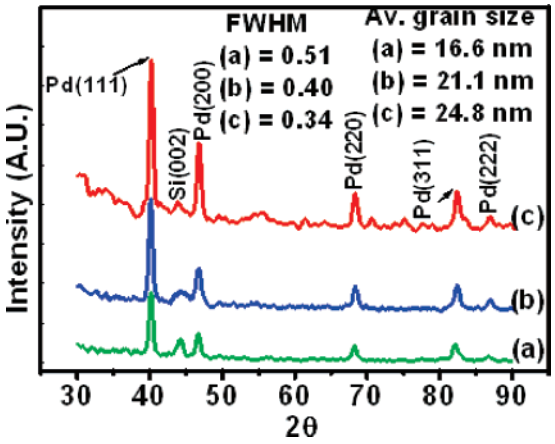

Figure 6. XRD patterns for the Pd nanoparticle grown on Si substrate using $PdCl_2$ + HCl mixture as electrolyte at the vias voltages of 0.1 V (a), 0.25 V (b), and 0.5 V (c).

area 240 $(nm)^2$ with average thickness of 15 nm. Nanostructures with nearly cubic shape, as shown in Figure 5c, were observed on the Si substrate while using the mixture of $Pd(NO_3)_2$ and HNO_3 as the electrolyte solution. This nitrate electrolyte results into the nanostructures of undefined shapes (Figure 5c′) on the W wire substrates using the electrochemical deposition. The above-mentioned variations in shape of nanoparticles show the importance of electrolyte solution and substrate in growth of the nanoparticles.

The electrochemical growth depends highly on the rate of reaction, density of ions in the solution, and their availability near the substrate. The presence of reacting ions in the solution is known to be effected by the nature of electrolyte solutions. The chemical solution deposition depends strongly on the ionic movement near the substrate surface. At a fixed applied electrode potential the ionic movement, which is dominantly responsible in determining the architecture of the deposited film particles, can either be changed by varying the dilution of the solution or by changing the nature of the solution. This is to say that the elementary shape of nanoparticles is determined by the initial nucleation rate, which depends on the ionic movement and ionic density near the surface, while the final size depends on the growth rate and the deposition time. Therefore, a variation in the shape of nanoparticles with changing the electrolyte solution can be obtained; on the basis of the nanoparticle requirement, an electrolyte can be selected for tailoring the nanoparticle shape and size.

Presence of only Pd in the nanoparticle films was observed by energy dispersive X-ray analysis. XRD has been used to analyze the crystallographic structure and average grain size for Pd nanoparticles grown on a Si substrate from the electrochemical deposition using different set of electrolyte solutions. Analysis of the XRD patterns (Figure 6) suggests the face-centered cubic (fcc) structure for the nanoparticles. The effect of increasing the bias voltage on the Si substrate during electrochemical deposition has been seen in terms of enhancement in the average grain size for the nanoparticles. Figure 6 shows the variation in average grain size, reflected from the peak broadening, for the nanoparticles grown from the mixture of $PdCl_2$ and HCl as electrolyte. Full width at half-maximum (fwhm) obtained form the peak broadening in XRD peaks was used to estimate the average crystallite size by using the Sherrer formula.[25]

2. Carbon Nanotubes. *(a) Surface Morphology.* Vertically aligned MWCNTs, as shown in Figure 7, were obtained on the Pd-coated Si substrates using the above set of optimized

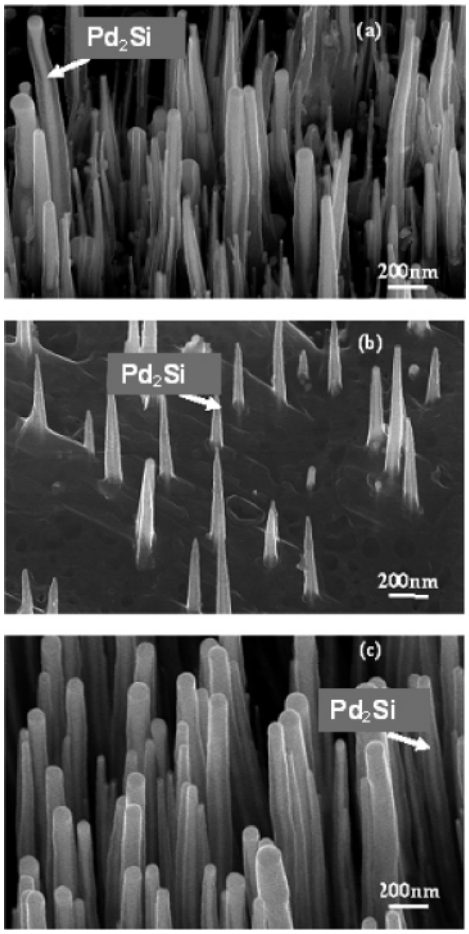

Figure 7. FESEM micrographs for MWCNT grown at identical MPECVD conditions on the Si substrate coated by Pd nanoparticles from $PdCl_2$ + HCl (a), $PdSO_4$ + H_2SO_4 (b), and $Pd(NO_3)_2$ + HNO_3 (c) electrolytes.

parameters in the MPECVD technique. The sizes and shapes of Pd particles have a significant role in determining the size and shape of MWCNTs on the Si substrates. The average size of Pd nanoparticles prior to CNT growth was estimated by using the peak broadening of XRD pattern. This is to mention that the possibility of changing the size and shape of the Pd particles just before the CNT growth cannot be ruled out completely. In our study, it was experimentally observed that the larger the size of Pd the shorter and thicker are the MWCNTs as compared to the MWCNTs obtained in the case of smaller Pd particles on the Si substrate. This was seen by growing the CNTs together on 4 substrates on which the average size of Pd particles was different. While all the growth parameters in MPECVD for all four Pd-coated substrates were the same so the observed variation on morphology of CNTs was believed to be due to the variation of initial shape and size of catalyst particles. This Pd shape- and size-dependent variation of the CNT morphology was observed for many sets of samples.

The growth of CNT is supported by the catalyst Pd through the decomposition of hydrocarbon molecules of a source gas followed by the adsorption of carbon atoms. HRTEM confirms the presence of graphite walls of a MWCNT. Figure 8 shows the typical HRTEM micrograph for the MWCNT prepared on the Pd-coated substrates in which the Pd was synthesized using the chloride electrolyte solution. The inset in the figure shows an enlarged picture to indicate the multiwalls of the CNTs. A HRTEM image was taken for the sample whose SEM image is shown in Figure 7a.

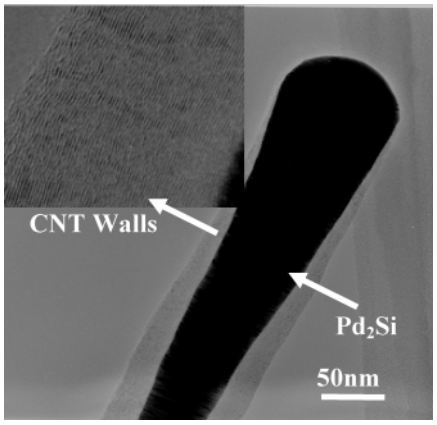

Figure 8. HRTEM micrograph for the MWCNTs prepared on the Pd-coated substrates in which the Pd particles were grown using $PdCl_2$ + HCl electrolyte solution. Inset in the figure shows the multiwalls of the CNTs.

The detailed TEM analysis has been reported in our earlier report. The interplanar distance (d) as estimated using HRTEM was found to be to be equal to ~0.57 nm. As discussed in our previous article,[21] we compare this calculated d value to the d values for the three most probable material structures under the present experimental conditions, which are PdO ($d_{(220)}$ = 0.20 nm, cubic, space group, $Fm3m$), Pd_2Si ($d_{(100)}$ = 0.563 nm, hexagonal, space group $P62m$) and $PdH_{0.649}$ ($d_{(110)}$ = 0.568 nm, cubic, space group $Pm3n$).[26] Thus, the possibility for the presence of PdO inside CNT is ruled out due to a significant difference in the d values for PdO (fcc structure) and the one calculated by TEM investigation. The d value of ~0.57 nm, is close to $d_{(110)}$ = 0.568 nm with body-centered cubic structure for $PdH_{0.649}$, and $d_{(100)}$ = 0.563 nm, hexagonal close-packed structure for Pd_2Si. In our previous article we discussed this issue and showed the possibility of $PdH_{0.649}$ and Pd_2Si. On the basis of the above results, it is difficult to say which one of these two materials is present inside the CNTs. We made attempts to solve this issue in this article. For this, we exposed the Pd nanoparticles to hydrogen in the same conditions used for CNT growth but in complete absence of any hydrocarbon gas to see the formation of Pd hydride, if possible due the high adsorption affinity of Pd toward hydrogen. This experiment was followed by the GAXRD measurements on these hydrogen-exposed Pd nanoparticles in order to see the structure of Pd-based materials. XRD pattern for these hydrogen exposed Pd particles is shown in Figure 9a. The observed peaks in the diffraction pattern have a good match with the standard peak positions for Pd_2Si; however, peaks for elemental Pd could also be seen in the XRD pattern. This study, therefore, confirms the presence of Pd_2Si inside the MWCNTs and the possibility of the presence of Pd hydride inside the MWCNT can be ruled out. Furthermore, the XRD pattern obtained for the Pd based material (Pd_2Si) filled CNTs also shows the presence of Pd_2Si inside the MWCNTs (Figure 9b).

Pd nanoparticles prepared using three different electrolyte solutions as mentioned before were used as catalyst for the growth of CNTs. The shape and size of CNTs are observed to be dominantly affected by the surface morphology of the base Pd nanoparticles prepared using different electrolyte solutions. The material filled inside the CNTs is marked in micrographs of Figure 7.

Parts a−c of Figure 5 are the SEM micrographs for the Pd nanoparticles resulting into the MWCNTs shown in parts a−c of Figure 7, respectively. The CNTs shown in Figure 7a were obtained from the catalyst particles in the shape of nanotriangles,

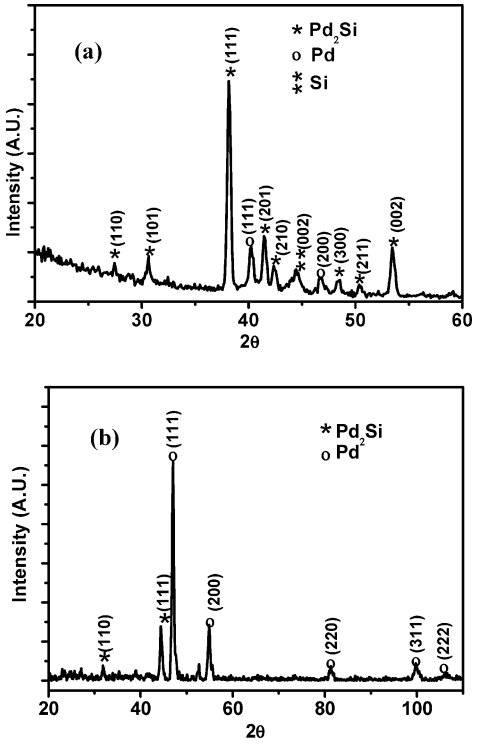

Figure 9. XRD patterns for (a) the hydrogen exposed Pd nanoparticles grown on Si substrate and (b) the MWCNTs.

nanocubes, and nanostars with the majority of shape structures as nanostars. This variation in size and shape, or in other words, particles of different shapes, of the catalyst is reflected on the morphology of CNTs (Figure 7a) in terms of CNTs with different sizes. On comparing the morphology of the CNTs shown in Figure 7, we suggest that the CNTs shown in Figure 7c to be the best so far observed by us. This is supported by the results of Raman spectroscopy, discussed later. We observed the CNTs with nearly of the same size, i.e., low polydispersity (Figure 7b), but "conical shaped", using the spherical shaped Pd catalyst particles of approximately monodisperse quality obtained using the sulfate electrolyte solution. By use of the cubical (or distorted cube) shaped Pd catalyst nanoparticles obtained by the nitrate electrolyte solution results in to the production of typical shaped carbon nanotubes filled with the Pd-based material, and thus considered good quality carbon nanotubes. The CNTs shown in Figure 7c have a low polydispersity compared to the CNTs shown in 7a. Therefore, based on the CNT morphogy, we suggest the cubical shaped Pd is observed to be a better catalyst than the spherical shaped Pd for the growth of carbon nanotubes by MPECVD. This was possibly due to the fact that a catalyst gains its active surface area on changing its shape from a sphere to the nonsphere.

The carbon nanotubes were also grown on the W tip, using the same parameters used for the CNT growth on Si. Parts a and b of Figure 10 show the morphology of the MWNTs grown on W tip. The catalyst Pd on W was grown using the nitrate electrolyte solution, and the Pd coated W tips were introduced in to the CVD chamber. Pd filled inside the MWCNT can be clearly seen on Figure 10a, which are the CNTs grown on the side of tip whereas the CNTs near to apex are shown in Figure 10b. Figure 10b is accompanied by an inset to show the CNT and W tip clearly. The inset is a low-resolution SEM micrograph for the same sample. The material inside the CNT is believed to be elemental Pd since the formation of silicide cannot occur in this case of using W substrate while the possibility of hydride formation has already been ruled in our experimental conditions.

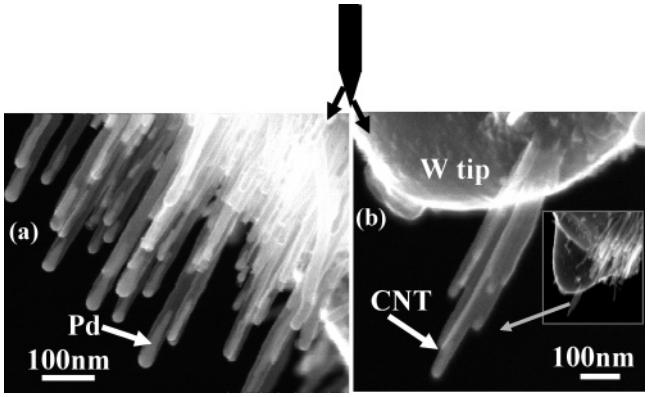

Figure 10. (a) and (b) show the FESEM pictures of the MWNTs grown on a W tip. The inside of the MWCNT filled with Pd can be in seen in figure (a); these are the CNTs grown on the side of tip, whereas the CNTs near to apex are shown in figure (b). The inset in (b) shows the low-resolution SEM micrograph for CNT on W tip.

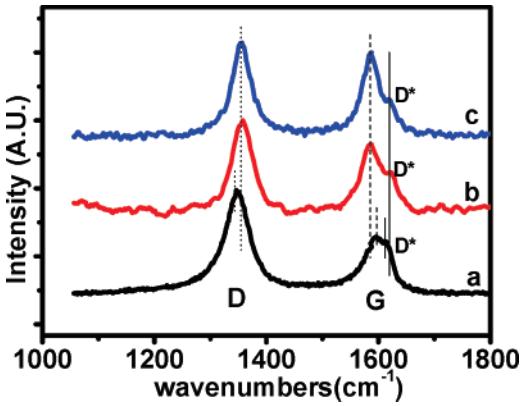

Figure 11. Plots of Raman spectroscopy for the MWCNT grown at identical MPECVD conditions on the Si substrate coated by Pd nanoparticles from $PdCl_2$ + HCl (a), $PdSO_4$ + H_2SO_4 (b), and Pd-$(NO_3)_2$ + HNO_3 (c) electrolytes.

This study shows the possible use of Pd-filled CNTs tips in scaning probe microscopy.

(b) Raman Spectroscopy. Raman spectra for the CNTs shown in parts a−c of Figure 7 are presented in Figure 11 as a, b, and c, respectively. The Raman spectroscopy is a nondestructive tool for characterization of carbon nanotubes. The typical Raman spectra for the CNTs consist of two quite sharp modes, the *G* peak around 1580 cm^{-1} and the *D* peak around 1350 cm^{-1} accompanied by an additional *D** peak as shoulder to the *G* peak at nearly 1610−1620 cm^{-1}. The *G* band, which is the characteristic of graphite phase, indicates the presence of crystalline graphite carbon in CNTs, whereas the *D* band is originated from the disorder induced features.[27] The presence of the *D** peak is attributed to the strong maximum in the vibrational density of states of graphite.[28] Referring to Figure 9 for plots b and c, the *G* band features at 1588 cm^{-1} (which is nearly same as graphite *G*-band frequency) with a shoulder at 1620 cm^{-1} is consistent with typical Raman *G* band frequencies reported for Pd-filled MWCNTs.[2] The disorder (*D*) mode at 1356 cm^{-1}, which is consistent with the *D* band reported, indicates the presence of amorphous carbon and suggests that there is a partial graphite coating on the catalyst particle. On comparing the peak position of spectra a in Figure 11 with spectra b and c, a shift in the position of all three Raman peaks for a can be easily noticed. The *G* peak has been shifted to 1595 cm^{-1}, while the *D* peak is shifted to 1346 cm^{-1}, accompanied by a shift in *D** to 1615 cm^{-1} for the MWCNTs. This shift in the peak positions, which is not clearly understood,

can possibly be attributed to the formation of different sized CNTs, shown in the SEM picture, for the sample a, whereas the CNTs for samples b and c, respectively, have less variation in size for a selected area of the sample. Also, the CNTs shown in a are thinner (on considering the average for a randomly selected area) in size compared to b and c; therefore, our results can be supported by the concept reported,[28] such as, a shift can be originated by structural change from graphite to nanocrystalline graphite. Following this analogy a peak shift can be expected on changing the CNT width from thick to thin. Moreover, the increase in frequency for graphite peak for the sample a suggests a decrease in the carbon−carbon distance for the nanotubes that can be correlated with the increase of conductivity for the carbon nanotubes shown in a as compared to the CNTs shown in b and c.

The ratio of intensities for *D* and *G* peak, I_D/I_G, for the three samples has been compared. This intensity ratio is generally considered as the parameter to characterize the quality of CNTs. The ratio (I_D/I_G) was observed to be minimum for the sample c and maximum for the sample a. This suggest that the CNTs in sample a, which has already shown the Raman peak shift with respect to b and c have a higher degree of disorder compared to the rest of two samples. The CNTs shown in Figure 7c, with minimum value of I_D/I_G ratio, are considered to be the best so far obtained by us. Raman spectroscopy data supports our suggestion based on SEM study for the quality of carbon nanotubes obtained using the Pd nanoparticles as catalyst.

Conclusions

An electrochemical method has been used to synthesize the Pd nanostructures on Si and W substrates with variation in shape and size. Different sets of electrolytes were used to achieve this variation in Pd nanoparticles. FESEM study shows the formation of well-defined Pd nanostructures with fcc structure as estimated by XRD. An increase in the size of the nanoparticles with an increase of bias voltage applied to the working electrode was noticed. MWCNTs have been synthesized by the MPECVD technique using the electrochemically grown Pd as catalyst. Growth of CNTs on the W tips has been demonstrated. Raman spectroscopy confirms the graphite nature of the carbon nanotubes. Efforts are continuously being made in the direction of synthesizing the CNT-coupled sharpened STM tips to realize it for actual applications.

Acknowledgment. We thank Mr. Seiji Shimabukuro and Prof. Takashi Ito of Gihu University, Japan, for their help in Raman spectroscopy measurement, and Dr. Suzuki of Semiconductors Laboratory, Toyota Technological Institute for XRD measurements. This work is supported by the "High Tech Research Center" project for private universities: matching fund subsidy from MEXT (Ministry of Education, Culture, Sports, Science and Technology), 2006−2008.

References and Notes

(1) Ho, P. F.; Chi, K. M. *Nanotechnology* **2004**, *15*, 1059.
(2) Hayashi, Y.; Tokunaga, T.; Toh, S.; Moon, W.-J.; Kaneko, K. *Diamond Relat. Mater.* **2005**, *14*, 790−793.
(3) Guella, G.; Zanchetta, C.; Patton, B.; Miotello, A. *J. Phys. Chem. B* **2006**, *110*, 17024.
(4) Corma, A.; Garcia, H.; Primo, A. *J. Catal.* **2006**, *241*, 123.
(5) Fukai, Y.; Sugimoto, H. *Adv. Phys.* **1985**, *34*, 263.
(6) Watari, N.; Ohnishi, S.; Ishii, Y. *J. Phys.: Condens. Matter* **2000**, *12*, 6799.
(7) Kishore, S.; Nelson, J. A.; Adair, J. H.; Eklund, P. C. *J. Alloy Compd.* **2005**, *389*, 234−242.
(8) Horinouchi, S.; Yamanoi, Y.; Yonezawa, T.; Mouri, T.; Nishihara, H. *Langmuir* **2006**, *22*, 1880.
(9) Anson, A.; Lafuente, E.; Urriolabeitia, E.; Navarro, R.; Benito, A. M.; Maser, W. K.; Martinez, M. T. *J. Phys. Chem. B* **2006**, *110*, 6643.
(10) Evans, J. *Chem. World* **2006**, *3*, 16.
(11) Korotcenkov, G.; Brinzari, V.; Boris, Y.; Ivanova, M.; Schwank, J.; Morante, J. *Thin Solid Films* **2003**, *436*, 119.
(12) Skala, T.; Veltruska, K.; Moroseac, M.; Matolinova, I.; Cirera, A.; Matolin, V. *Surf. Sci.* **2004**, *566*, 1217.
(13) Suda, Y.; Kawasaki, H.; Namba, J.; Iwatsuji, K.; Doi, K.; Wada, K. *Surf. Coat. Technol.* **2003**, *174*, 1293.
(14) Toh, S.; Kaneko, K.; Hayashi, Y.; Tokunaga, T.; Moon, W. J. *J. Electron Microsc.* **2004**, *53*, 149.
(15) Lu, Y. J.; Li; J.; Han, J.; Ng, H. T.; Binder, C.; Partridge, C.; Meyyappan, M. *Chem. Phys. Lett.* **2004**, *391*, 344.
(16) Kilber, L. A.; Kleinert, M.; Kolb, D. M. *Surf. Sci.* **2000**, *461* 155.
(17) Ball, M. J.; Lucas, C. A.; Markovic, N. M. Stamenkovic, V.; Ross, P. N. *Surf. Sci.* **2003**, *518*, 201.
(18) Ball, M. J.; Lucas, C. A.; Markovic, N. M. Stamenkovic, V.; Ross, P. N. *Surf. Sci.* **2003**, *540*, 295.
(19) Guo, D.-J.; Li, H.-L. *Electrochem. Commun.* **2004**, *6*, 999.
(20) Shekhah, O.; Busse, C.; Bashir, A.; Turcu, F.; Yin, X.; Cyganik, P.; Birkner, A.; Schuhmann, W.; Woll, C. *Phys. Chem. Chem. Phys.* **2006**, *8*, 2257.
(21) Joshi, R. K.; Yoshimura, M.; Matsuura, Y.; Ueda, K.; Tanaka, K. *J. Nanosci. Nanotechnol.* **2007**, *7*, 4272−4277.
(22) Tanaka, K.; Yoshimura, M.; Okamoto, A.; Ueda, K. *Jpn. J. Appl Phys.* **2005**, *44*, 2076−2078.
(23) Yoshimura, M.; Tanaka, K.; Ueda, K. *Jpn. J. Appl Phys.* **2005**, *44*, 1562−1563.
(24) Bera, D.; Kuiry, S. C.; Seal, S. *J. Phys. Chem. B* **2004**, *108* 556−562.
(25) Cullity B. D. *Elements of X-Ray Diffraction*; Addison Wesley: New York, 1967.
(26) Kennedy, S. J.; Wu, E.; Kisi, E. H.; Gray, E. M.; Kennedy, B. J. *J. Phys.: Condens. Matter* **1995**, *7*, L 33−L 40.
(27) Delhaes, P.; Couzi, M.; Trinquecoste, M.; Dentzer, J.; Hamidou, H.; Vix-Guterl, C. *Carbon* **2006**, *44*, 3005−3013.
(28) Ferrari, A. C.; Robertson, J. *Phys. Rev.* **2000**, *61*, 14095−14107.